Seismic precursors linked to super-critical fluids at oceanic transform faults

Citation	Géli, L., Piau, J. M., Dziak, R., Maury, V., Fitzenz, D., Coutellier, Q., & Henry, P. (2014). Seismic precursors linked to super-critical fluids at oceanic transform faults. Nature Geoscience, 7(10), 757-761. doi:10.1038/ngeo2244
DOI	10.1038/ngeo2244
Publisher	Nature Publishing Group
Version	Version of Record
Terms of Use	http://cdss.library.oregonstate.edu/sa-termsofuse

nature geoscience

LETTERS

PUBLISHED ONLINE: 14 SEPTEMBER 2014 | DOI: 10.1038/NGEO2244

Seismic precursors linked to super-critical fluids at oceanic transform faults

Louis Géli[1]*, Jean-Michel Piau[2], Robert Dziak[3], Vincent Maury[4,5], Delphine Fitzenz[6], Quentin Coutellier[1,7] and Pierre Henry[8]

Large earthquakes on mid-ocean ridge transform faults are commonly preceded by foreshocks[1–3] and changes in the seismic properties of the fault zone[3]. These seismic precursors could be linked to fluid-related processes[2,3]. Hydrothermal fluids within young, hot crust near the intersection of oceanic transform faults are probably in a supercritical condition[4]. At constant temperature, supercritical fluids become significantly more compressible with decreasing pressure, with potential impacts on fault behaviour. Here we use a theoretical model to show that oceanic transform faults can switch from dilatant and progressive deformation to rupture in response to fluid-related processes. We assume that the fault core material behaves according to a Cam-clay-type[5] constitutive law, which is commonly used to account for the behaviour of clays. According to our model, we find that the fault is initially stable, with stresses gradually increasing over a timescale of years in response to tectonic loading. The fault evolves into a metastable phase, lasting a few days, during which the fault rocks dilate and pore pressures decrease, causing the compressibility of the supercritical fluids to increase. This in turn triggers fault-slip instability that creates foreshock swarms. In the final phase, the fault fails in the mainshock rupture. Our results imply that seismic precursors are caused by changes in fluid pressure which result in variations in fluid compressibility, in response to rock deformation just before rupture.

The seismogenic character of oceanic fracture zones has been the subject of debate over the past three decades. Early work showed the anomalously large excitation of long-period waves by ocean transform earthquakes[6,7], and that some transform earthquakes exhibit long-period seismic anomalies that are best explained by episodes of slow, smooth deformation, several hundred seconds before the high-frequency origin time[8]. The possibility of anomalously slow rupture preceding the normal speed rupture could be useful for short-term prediction. However, errors and approximations in the centroid depth, focal mechanism and earth structure at the source may have significant effects on the shape of the source spectra[9,10]. Hence, the previously proposed slow rupture components could be simply explained as artefacts generated by the modelling procedure.

Results obtained with hydrophone arrays moored in the Sound Fixing and Ranging (SOFAR) channel, which allow locating seafloor earthquakes at epicentral distances of thousands of kilometres, through the detection of tertiary (T-) waves scattered at the seafloor[11], have further confirmed that the seismicity at oceanic transform faults exhibits characteristics different from those of continental transforms[1,2]. A paramount example was a sequence of precursors, documented on 2 June 2000, before a M_w 6.2 earthquake that occurred at the Blanco Fault Zone (FZ), near the intersection with the Juan de Fuca Ridge off the coast of the northwestern USA (Fig. 1). During the 12 hours preceding the mainshock, a total of 72 hydro-acoustically detected earthquakes were recorded on the sound surveillance system (SOSUS) hydrophone arrays. Most foreshocks were clustered near the epicentre, whereas aftershocks were aligned along a fault plane (this observation is within location error). It is worth noting here that the temperature of two nearby hydrothermal vents located on the axis of the Juan de Fuca Ridge, <39 km away from the epicentre, decreased by ~3 °C and 14 °C during the 17 and 60 days, respectively, that preceded the mainshock[1].

A second example of clear foreshock behaviour was also observed during detailed analysis of ocean-bottom seismometer (OBS) data from the Gofar Transform Fault (East Pacific Rise)[3]. A swarm of approximately 20,000 foreshocks occurred in a 10-km-long confined region during the seven days that preceded a M_w 6.0 earthquake which occurred on 18 September 2008. Clear variations in seismic velocities (V_P and V_S) were observed at the Gofar FZ, both temporally and spatially. The foreshock area was found to undergo a 3% decrease in average shear-wave speed during the week preceding the mainshock. Moreover, the differences in S and P wave arrival times ($t_S - t_P$) for vertically propagating waves are much greater (by 50–100%) in the foreshock region than within the rupture area. Furthermore, the V_P/V_S ratio in the lower crust seems typical of oceanic crust, whereas low P-wave velocities were found throughout the foreshock zone, using coda measurements which are most sensitive to the shallow (~0–3 km) section

Seismological and geodetic work conducted at major continental transform faults on land have shown that low-velocity 'damage zones', a few hundred to a few thousand of metres wide, could extend a few kilometres into the crust[12–14]. A significant permeability contrast, of three to five orders of magnitude, exists between these damage zones and the surrounding rock[15]. Swath bathymetry and side-scan sonar images of oceanic transforms show that there is generally not one single fault, but a number of 'faulting systems'

[1]Ifremer, Marine Geosciences Department/Institut Carnot Ifremer-EDROME, BP 70, 29280 Plouzané, France, [2]Department of Materials and Structures (MAST), IFSTTAR, Centre de Nantes, CS4, 443444 Bouguenais Cedex, France, [3]Cooperative Institute for Marine Resource Studies/Oregon State University; Pacific Marine Environmental Laboratory/National Oceanic and Atmospheric Administration, Hatfield Marine Science Center, Newport, Oregon 97365, USA, [4]Université Montpellier II, Géosciences Montpellier, Place Eugène Bataillon, 34000 Montpellier, France, [5]IFP School, 228-232 Av. Napoléon Bonaparte, 92852 Rueil-Malmaison, France, [6]RMS, 7575 Gateway Blvd, Newark, California 94546, USA, [7]ENIB, Parvis Blaise Pascal, 29280 Plouzané, France, [8]CEREGE, Aix-Marseille Université, BP 80, 13545 Aix en Provence Cedex 04, France. *e-mail: louis.geli@ifremer.fr

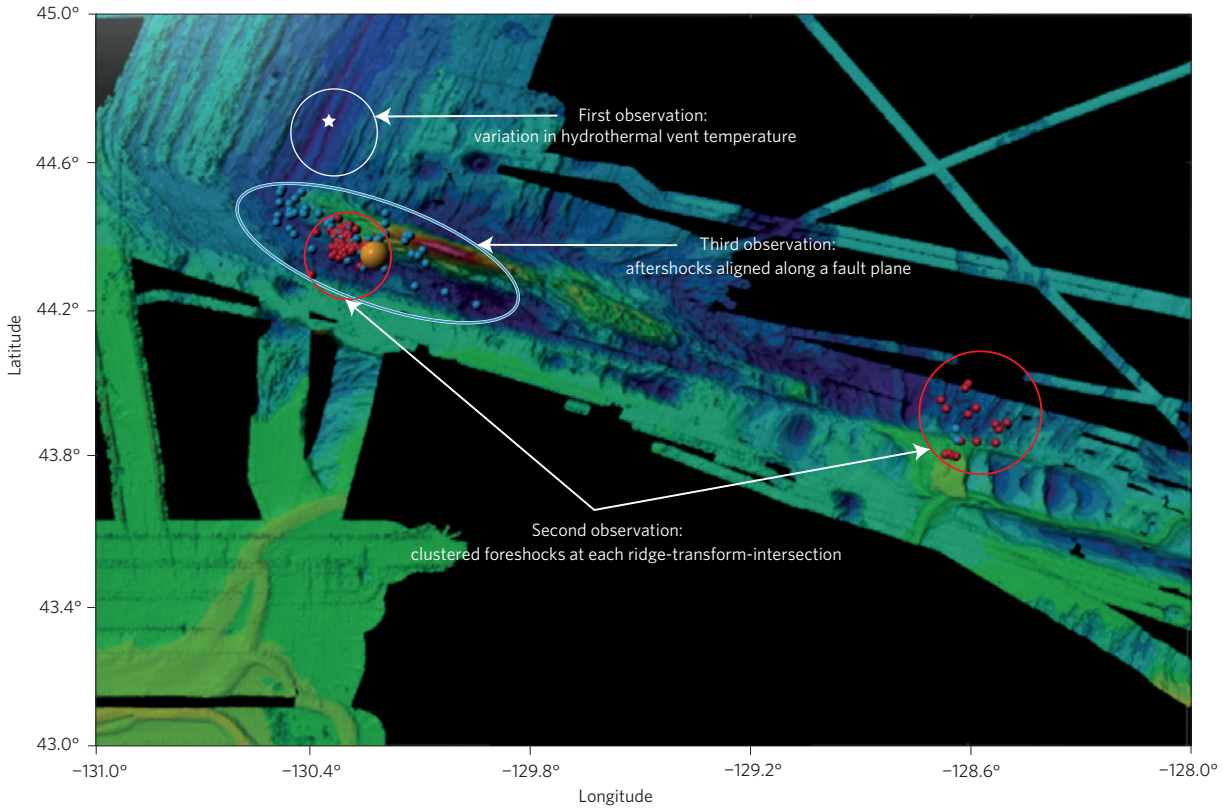

Figure 1 | Seismic sequence related to the Blanco, 6.2 M_w earthquake of June 2000. Bathymetry of the Blanco FZ with precursors (red dots) and aftershocks (blue dots) related to the mainshock (yellow dot). The white star indicates the location of the temperature measurements at two hydrothermal vent sites, reported in ref. 1. The Blanco Transform is a 350-km-long strike-slip fault that comprises five major right-stepping fault segments offset by deep extensional basins[24]. Traces of intense alteration[25] from the epicentre area indicate the existence of an active hydrothermal circulation within the fault zone through open cracks on the seafloor.

consisting of parallel faults, sometimes separated by pull-apart basins, due to tensional components that widen the transform valley. As a result, water penetrates into transform faults, not only through the main active fault, but also through a number of fault segments, each having a so-called 'damage' zone, a few hundreds of metres wide, and a common root at depth. It is expected that within 'warm' oceanic transform faults, or near ridge-transform intersections, temperatures of a few hundred °C are found, hence super-critical conditions are probably a few kilometres below the seafloor (see Fig. 2 and Supplementary Appendix 1a). Within the super-critical domain, the compressibility increases significantly in a nonlinear way (Fig. 3), whereas both the density and the viscosity decrease.

Hereafter we propose a theoretical, poro-mechanical model that describes how such pronounced changes may affect the fault behaviour and therefore consistently explain the observations. The model, known as the Piau–Maury–Fitzenz (PMF) model, was originally developed[16] to study the role of highly compressible fluids on faulting, and is fully described in Supplementary Appendix 2. The schematic geometry shows a fault core surrounded by two sections of bedrock (pads P) with finite width, subject to anti-symmetric far-field tectonic displacements on their outer boundaries (Fig. 4a), essentially in shear mode. The two bedrock segments are considered as non-porous elastic media, whereas the fault core material is supposed to have a poro-rigid-plastic constitutive law of Cam-clay-type[5,17]. This plasticity model is well known in soil mechanics as being able to account for both the contraction/hardening and the dilatant/softening behaviour of clay soils, depending on their state of consolidation (void content) and the applied (effective) stresses. Our choice was guided by the observed behaviour of geological faults, which also can exhibit either contraction or dilatant strain modes. However, to simplify computation of the model, we assume the thickness of the fault core is negligible compared to that of the bedrock. This is believed to be a simple way to represent the transition from non-localized to localized modes of strain along faults as a function of their maturity.

This leads us to transpose the volumetric Cam-clay constitutive law into an original interface standard poro-plastic constitutive law (I), which inherits the main features of the three-dimensional formulation that is commonly used in soil mechanics[5,17,18]. The pore pressure evolves within the fault core in relation to both the interface dilatancy via the fluid compressibility and a possible link with an external source of pressure. In our modelling approach, dilatancy is related to the discontinuity of the normal displacement at the interface.

Compared to models based on the rate- and state-dependent friction laws that are more commonly used in earthquake science[19–21], the interface model (I) proposed here presents certain advantages. It avoids any consideration about rate-dependent friction phenomena and makes use of standard plasticity concepts to couple hardening/softening aspects with dilatant and shear displacements. As a result, the potential number of model parameters is rather small—each having a straightforward physical interpretation—which facilitates the choice of their numerical values.

One important feature shown by the model (pads + interface) is the competition between mechanical softening and hydraulic stiffening. In dilatant, undrained conditions, the softening of the fault core material (expressed through the behaviour law of the interface) is counterbalanced, within some limits, by a 'stiffening'

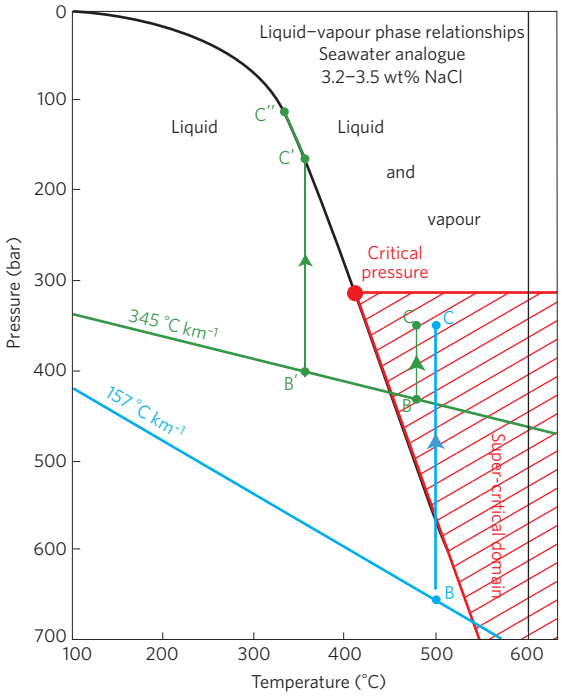

Figure 2 | Phase diagram of seawater (3.2–3.5 wt% NaCl)[4,26]. Within the Blanco FZ (blue line) the geotherm (157 °C km^{-1}) is computed in 0.75 Myr-old crust, using commonly accepted values for cooling plate models[27] and a zero-age seafloor depth of 3,500 m (Supplementary Appendix 1b). Within the Gofar FZ (green line) the geotherm (345 °C km^{-1}) is for 0.15 Myr-old crust and a seafloor depth of 3,000 m. At point B, fluid pressure starts to decrease isothermally in response to dilatancy. Near C, fluid compressibility increases markedly, triggering the metastable phase described in the text. In very young, hot crust, the temperature–pressure path may also follow the line from B′ to C′, where vaporization occurs, then from C′ to C″ along the transition curve.

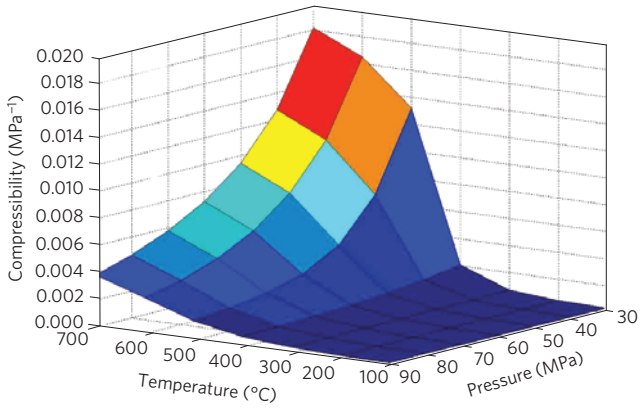

Figure 3 | Variations in water compressibility with temperature and pressure. The computations presented here are based on the National Institute of Standards and Technology (NIST) WebBook[28].

effect due to the decrease in pore pressure (and to the subsequent increase in the normal effective stress). In drained conditions, this competition still persists, because at some point dilatancy is found to evolve more rapidly than hydraulic diffusion.

As a consequence of the competition between these two opposing effects, three domains appear in the σ_n'–τ plane (Fig. 4), depending on the relative importance of stiffening versus hardening. These three domains are strongly related to the properties (particularly to the compressibility) of the fluid and characterized by different timescales, ranging from years to seconds. In the first, stable domain, the stress path evolves on the scale of years in response to tectonic loading. In the second, metastable domain, the stress path evolves on the scale of days in response to fluid-related processes. In the third, unstable domain, there is no analytical solution to the model equations, unless inertial forces are introduced. In this case the solution is found to evolve on the scale of a few seconds, with large displacements, describing the mainshock.

Here we apply the model to the situation of the oceanic faults described above, using adequate parameters. A slight divergent far-field component is applied in addition to tectonic shear displacements. Model computation results are illustrated by the stress path ABCDEF (Fig. 4b,c).

From A to C, the stress path evolves in the stable domain and in response to the tectonic loading. From A to B, the solution evolves in the elastic domain and no displacement occurs at the interface. The total normal stress decreases, whereas the pore pressure is kept constant within the fault, which results in a decreasing normal effective stress. At point B, the stress path hits and then follows the criterion, while dilatancy is initiated. Along BC, dilatancy progressively increases and the criterion evolves slightly, as expected from the Cam-clay model. In undrained conditions, the pore pressure decreases with dilatancy. The decrease in pore pressure is here found to be more intense than the decrease of the amplitude of the total normal stress. Consequently, the amplitude of the effective normal stress increases. In that phase, however, the low compressibility of the fluid (taken equal to 10^{-4} MPa^{-1} in Fig. 4b) limits the evolution of dilatancy and, consequently, the evolution of the size of the fault criterion.

At point C, the pore pressure is such that the fluid compressibility starts to increase significantly, based on the PVT diagram in the super-critical domain, triggering a phase of metastability, CD, followed by a phase of instability. The controlling factors during this phase are mostly related to the fluid properties. Along CD, the stress conditions in the fault core evolve rapidly with characteristic timescales of a few days. This metastable phase is considered as being related to the period of foreshocks, observed at Blanco and Gofar. In the Gofar foreshock swarm area, the temperature–pressure conditions may be near critical (Fig. 2 and Supplementary Appendix 2). Close to the critical point, the transition from liquid to vapour results in particularly strong changes in fluid compressibility (which may tend to infinity), which are expected to produce enhanced effects with regards to the model.

At point D, the stress path gets closer to the summit of the criterion ellipse. Consequently the dilatancy and stiffening effects become less active, as expected from the Cam-clay constitutive law of the fault core material. Hence, the softening of the material has no more hardening counterpart. The stress path evolves along DEF in a few seconds, under the control of inertial forces developed in the surrounding bedrock that trigger elastic waves within the pads (Supplementary Appendix 2).

On the basis of the above analysis, the foreshock sequence observed at both the Blanco and the Gofar fracture zones are believed to correspond to the metastable phase along CD, which precedes the main shock represented by the segment DEF. Foreshocks are thus likely to be restricted to areas where super-critical (or near-critical, which implies the possible occurrence of vapour) conditions are present. Model calculations of wave propagation in fluid-saturated, porous media (Supplementary Appendix 3) indicate that both V_P and V_S decrease significantly when the (dilatancy-related) porosity increases, whereas the V_P/V_S ratio remains within reasonable bounds (between 1.79 and 1.83), representative of 'typical oceanic crust'. As a result, the difference in seismic wave arrival times (t_S-t_P) observed at the Gofar FZ require both low P and low S velocities. The foreshock region at the Gofar FZ might thus not be as deep as

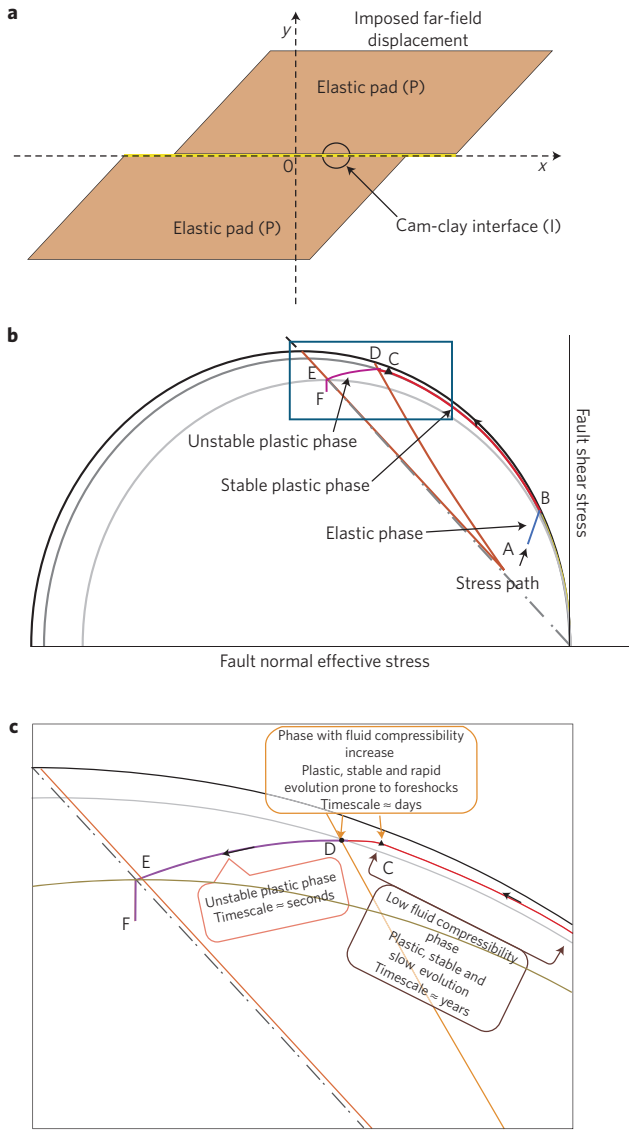

Figure 4 | Stress path scenario for Gofar and Blanco faults, inferred from the PMF model. a–c, Model geometry (**a**) and stress-path evolution within the interface: general view (**b**) and enlargement (**c**). From A to C, the stable path evolves under tectonic loading, with a timescale of (tens of) years. AB = elastic evolution, BC = plastic dilatant evolution. From C to D, the stress path evolves into a metastable plastic domain, triggered by an increase in fluid compressibility. From D to F, the evolution is unstable, with characteristic timescales of a few seconds. The curvilinear domain between the orange curves and the path towards point F are explained in detail in Supplementary Appendix 2.

previously proposed[3], but confined within the upper 3 km, where both low P-velocity waves and low S-velocity waves were found. In contrast, the observation that the temperature of the hydrothermal vents 39 km away decreased several weeks before the Blanco main-shock epicentre does not as yet have a clear explanation. Although a causal relation with the earthquake occurrence cannot be precluded (see Supplementary Appendix 1b and refs 22,23), the lack of further temperature measurements prevents us from going any further into the discussion.

The metastable phase described in this paper has been shown to occur in response to changes in fluid properties in very young crust within oceanic transform faults. Such environments are characterized by very high geothermal gradients, which are not commonly found elsewhere on Earth. Still, the work presented here may help improve the general understanding of earthquake processes in submarine environments—particularly at subduction zones, where the role of fluids is recognized, but not understood. Furthermore, recognition of the role of super-critical fluids on faulting may have broad implications, not just at transform faults, but potentially also throughout the mid-ocean ridge system and in high heat flow, fluid-rich continental faulting environments.

Received 30 January 2014; accepted 8 August 2014; published online 14 September 2014

References

1. Dziak, R. P., Chadwick, W. W. Jr, Fox, C. G. & Embley, R. W. Hydrothermal temperature changes at the Southern Juan de Fuca Ridge associated with M_w 6.2 Blanco transform earthquake. *Geology* **31,** 119–122 (2003).
2. McGuire, J. J., Boettcher, M. S. & Jordan, T. H. Foreshock sequences and short-term earthquake predictability on East Pacific Rise transform faults. *Nature* **434,** 457–461 (2005).
3. McGuire, J. J. *et al.* Variations in earthquake rupture properties along the Gofar transform fault, East Pacific Rise. *Nature Geosci.* **5,** 336–341 (2012).
4. Bischoff, J. L. & Rosenbauer, R. J. An empirical equation of state for hydrothermal seawater (3.2 percent NaCl). *Am. J. Sci.* **285,** 725–763 (1985).
5. Roscoe, K. H. & Burland, J. B. *On the Generalized Stress–Strain Behavior of 'Wet' Clay* 535–609 (Cambridge Univ. Press, 1968).
6. Kanamori, H. & Stewart, G. S. Mode of the strain release along the Gibbs fracture zone, Mid-Atlantic ridge. *Phys. Earth Planet. Inter.* **11,** 312–332 (1976).
7. Okal, E. A. & Stewart, L. M. Slow earthquakes along oceanic fracture zones: Evidence for asthenospheric flow away from hotspots? *Earth Planet. Sci. Lett.* **57,** 75–87 (1982).
8. Ihmlé, P. & Jordan, T. H. Teleseismic search for slow precursors to large earthquakes. *Science* **266,** 1547–1551 (1994).
9. Abercombrie, R. & Ekström, G. Earthquake slip on oceanic transform faults. *Nature* **410,** 74–77 (2001).
10. Abercombrie, R. & Ekström, G. A reassessment of the rupture characteristics of oceanic transform earthquakes. *J. Geophys. Res.* **108,** 2225 (2003).
11. Fox, C. G., Dziak, R. P., Matsumoto, H. & Schreiner, A. E. Potential for monitoring low-level seismicity on the Juan de Fuca Ridge using military hydrophone arrays. *Mar. Technol. Soc. J.* **27,** 22–30 (1994).
12. Ben-Zion, Y. *et al.* A shallow fault-zone structure illuminated by trapped waves in the Karadere-Duzce branch of the North-Anatolian Fault, Western Turkey. *Geophys. J. Int.* **152,** 699–717 (2003).
13. Fialko, Y. Probing the mechanical properties of seismically active crust with space geodesy: Study of the coseismic deformation due to the 1992 M_w 7.3 Landers (South California) earthquake. *J. Geophys. Res.* **109,** 1–19 (2004).
14. Peng, Z. *et al.* Quantitative analysis of seismic fault zone waves in the rupture zone of the 1992 Landers, California, earthquake: Evidence for a shallow trapping structure. *Geophys. J. Int.* **155,** 1021–1041 (2003).
15. Lockner, D. *et al. Permeability and Strength of Core Samples for the Nojima Fault of the 1995 Kobe Earthquake.* Report No. 0F 00-0129 147–152 (US Geological Survey, 2000).
16. Maury, V., Piau, J-M. & Fitzenz, D. in *Harmonising Rock Engineering and the Environment* (*12th ISRM Internat. Congress on Rock Mechanics Beijing Oct. 2011*) (eds Qian, Q. & Zhou, Y.) (CRC Press, 2011); available at http://dx.doi.org/10.13140/2.1.1077.1849.
17. Roscoe, K. H., Schofield, A. N. & Wroth, C. P. On the yielding of soils. *Geotechnique* **8,** 22–53 (1958).
18. Schofield, A. N. & Wroth, C. P. *Critical State Soil Mechanics* (McGraw-Hill, 1968).
19. Dieterich, J. H. Time dependent friction and the mechanics of stick-slip. *Pure Appl. Geophys.* **116,** 790–806 (1978).
20. Ruina, A. Slip instability and state variable friction laws. *J. Geophys. Res.* **88,** 10359–10370 (1983).
21. Segall, P. Rice, Dilatancy, compaction and slip instability of a fluid infiltrated fault. *J. Geophys. Res.* **100,** 22155–22171 (1995).
22. Davis, E. E. *et al.* Hydrological response to a sea-floor spreading episode of the Juan de Fuca Ridge. *Nature* **430,** 335–338 (2004).
23. Guéguen, Y. & Palciauskas, V. *Introduction à La Physique Des Roches* 299 (Hermann, Paris, 1992).
24. Embley, R. W. & Wilson, D. S. Morphology of the Blanco Transform Fault, northeast Pacific. Implications for its tectonic evolution. *Mar. Geophys. Res.* **14,** 25–45 (1992).
25. Juteau, T. *et al.* A submersible study in the Western Blanco fracture zone: Structure and evolution during the last 1.6 Ma. *Mar. Geophys. Res.* **17,** 399–430 (1995).

26. Koshinsky, *et al.* Hydrothermal venting at pressure–temperature conditions above the critical point of seawater, 5° S on the Mid-Atlantic Ridge. *Geology* **36,** 615–618 (2008).
27. Parsons, T. & Sclater, J. An analysis of ocean floor bathymetry and heat flow with age. *J. Geophys. Res.* **82,** 803–827 (1977).
28. Lemmon, E. W., McLinden, M. O. & Huber, M. L. NIST Reference Fluid Thermodynamic and Transport Properties—REFPROP, Version 7.0. *NIST Standard Reference Database 23* (NIST, 2002).

Acknowledgements

This work is a tribute to late Jean Francheteau, who passed away on 21 July, 2010. Jean supported the ideas developed in this paper since the very beginning. The work was initiated in 2005, when L.G. was a Cecil and Ida Green Scholar at IGPP/SIO, University of California, San Diego, at the invitation of J. Orcutt and M. Zumberge, who are both greatly acknowledged here. Discussions with Y. Fialko, Y. Hamiel and J. Sclater were very useful. This paper is NOAA/PMEL contribution number 4109.

Author contributions

L.G. initiated the work based on previous work by R.D., who provided the initial dataset from the Blanco FZ and greatly contributed to the ideas developed in the manuscript. L.G. and P.H. discussed different models, before employing the Piau–Maury–Fitzenz model, produced by J-M.P., V.M. and D.F. J-M.P., V.M. and L.G. worked on the application of the model to the Blanco FZ. J-M.P. wrote Supplementary Appendix 2. L.G. wrote Supplementary Appendix 3, with contributions from Q.C. and V.M. All authors discussed results and contributed to the manuscript.

Additional information

Supplementary information is available in the online version of the paper. Reprints and permissions information is available online at www.nature.com/reprints. Correspondence and requests for materials should be addressed to L.G.

Competing financial interests

The authors declare no competing financial interests.